NASA TECHNICAL NOTE

NASA TN D-5168
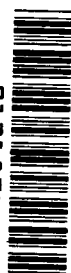
NASA TN D-5168

VARIATION OF CONVECTIVE HEAT-TRANSFER COEFFICIENT AROUND A SIMULATED ROCKET COOLING TUBE SECTION

by Ronald G. Huff

Lewis Research Center

Cleveland, Ohio

VARIATION OF CONVECTIVE HEAT-TRANSFER COEFFICIENT

AROUND A SIMULATED ROCKET COOLING TUBE SECTION

By Ronald G. Huff

Lewis Research Center
Cleveland, Ohio

NATIONAL AERONAUTICS AND SPACE ADMINISTRATION

ABSTRACT

An experiment was performed using an insulated pipe through which hot air flowed. The pipe wall was made of tubes having a semicircular cross section which simulates the geometry found in many rocket engines. The peripheral variation of the convective heat-transfer coefficient between the gas and the tubes was measured for one of the tubes. It was found that the coefficient is equal to the coefficient at the crest of the tube times the cosine of the angle measured from the crest.

VARIATION OF CONVECTIVE HEAT-TRANSFER COEFFICIENT

AROUND A SIMULATED ROCKET COOLING TUBE SECTION

by Ronald G. Huff

Lewis Research Center

SUMMARY

Boundary layer interaction between adjacent circular or semicircular cooling tubes in rocket engines tends to lower convective heat-transfer coefficients between the tubes. To determine the effect of this interaction on the coefficient, an experimental program was initiated using an insulated pipe with walls made of tubes having a semicircular cross section representing the rocket wall. Heated air flowed through the pipe. The tube to tube inside diameter of the pipe was 4.37 inches (0.111 m). The tube diameter was 5/8 inch (0.01588 m). The Reynolds number was 1.786×10^6; the Nusselt number was 2372 based on pipe diameter; and the Prandtl number was 0.676. This adiabatic model was intended to give a first-order approximation to the more complicated case of the rocket engine where the wall temperature varies in the peripheral direction and the variation of the convective heat transfer coefficient due to the boundary layer interaction can be affected by the cooling of the boundary layer between the cooling tubes.

The variation of the convective heat-transfer coefficient found in the experiment followed a cosine curve with angular peripheral location. The maximum value was located at the crest of the tube which represented the rocket cooling tube. This cosine distribution allows the use of the projected area of the tube along with the heat-transfer coefficient at the crest of the tube when calculating the heat flux to the coolant. This statement assumes that the large temperature differences between the rocket gases and wall temperature makes the variation of the wall temperature negligible when calculating the heat flux to the rocket coolant or that heat flux is calculated after having used the cosine variation of the coefficient to calculate the surface wall temperature distribution.

INTRODUCTION

Gas-side heat-transfer experiments have been conducted in the past with smooth wall rocket engines (ref. 1). These experiments have determined the variation of heat

transfer in the axial direction. Conventional rocket engines, however, generally do not have smooth walls but use cooling tubes that have a semicircular cross section. A rocket engine of this type is shown in figure 1.

The enlarged view (fig. 1) of a cross section of the rocket engine shows that a wall made of semicircular cooling tubes presents a corrugated surface to the combustion gases (gas flow parallel to the corrugations). The variation of the convective heat-transfer coefficient across these corrugations has not been studied experimentally.

An analytical investigation has been performed by Deissler (ref. 2) on a heat exchanger having banks of tubes which are tangent to one another with fluid flowing between the tubes in the axial direction. The analysis was performed for turbulent flow. It indicated that the heat-transfer coefficient should approach zero at the point where the tubes are tangent and should be a maximum value at the crest.

The purpose of this experimental investigation, which was conducted at the Lewis Research Center, was to measure the variations of the gas-side convective heat-transfer coefficient across a thermally insulated corrugated surface that represented the tubular walls of a cooled rocket engine. The resulting variation in coefficient can then be applied as a boundary condition when calculating the rocket wall temperature distribution. When
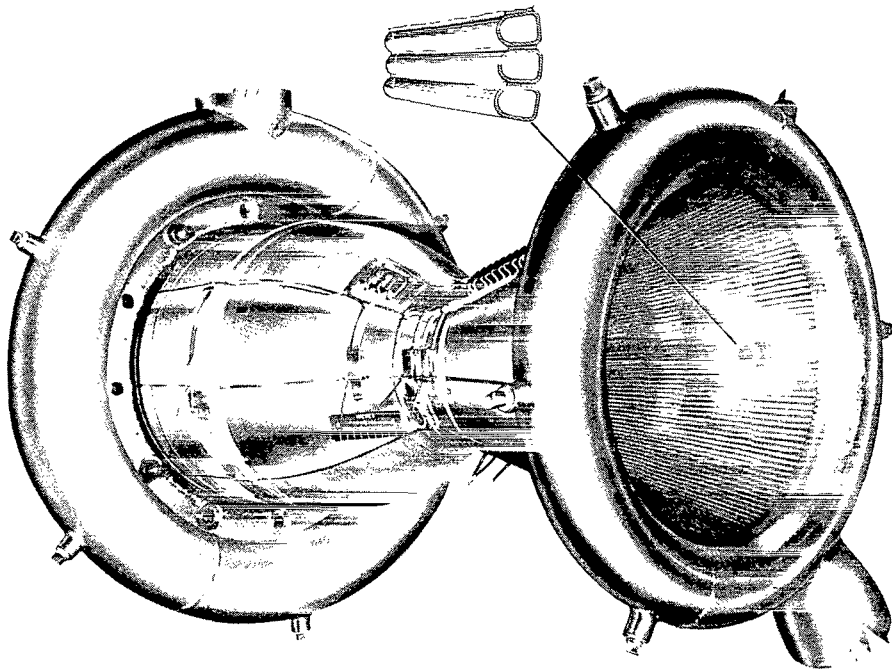
CD-9934-14

Figure 1. - Rocket engine having interior wall of semicircular cooling passages (corrugated interior surface).

the wall temperatures and the coefficients are known, the heat flux to the coolant can be calculated.

This experiment is not intended to determine the effect of cooling of the hot gases between the rocket cooling tubes on the distribution of the coefficients. It also does not account for the axial changes in geometry which are present in rocket engines.

The method used to determine the convective heat-transfer coefficient h is developed in reference 3. It consists in this case of sinusoidally oscillating the temperature of the air flowing through the insulated test section and measuring the response of the wall temperature. The phase lag between the air and wall temperatures along with the wall properties (i.e., density, specific heat, thermal conductivity) and frequency of the air temperature oscillations can be used to calculate the convective heat-transfer coefficient h.

APPARATUS

The experimental apparatus is shown in figure 2. Air was passed through a combustor in which hydrogen was used as the fuel in order to minimize contamination of the air. The resulting combustion products, air plus water vapor, then passed into a mixing chamber and from there into the test section. The mass flow rate through the test section was controlled by a choked, variable area nozzle located at the end of the test section.

The hydrogen mass flow rate and hence temperature of the air was controlled by a pneumatic operated valve which had a linear area variation with stroke. The hydrogen mass flow rate was limited to less than 1 percent of the total mass flow rate. The position of the valve was controlled by an electric to pneumatic signal converter. The electrical input to the converter came from a sine wave generator in series with a voltage divided circuit which was used to set the average hydrogen flow rate.

The details of the combustor are shown in figure 3. Air was supplied through a pipe located at the top of the combustor. It then was turned 90° by a baffle plate and flowed through a perforated plate. Hydrogen was injected into the stream through three closed end perforated tubes which had roof type shields on the upstream side. The shield acts as a flame holder. The hydrogen injectors were arranged parallel and located just under the perforated plate. Combustion takes place here and mixing occurs as the air was turned again 90° and enters a mixing chamber. Ignition of the hydrogen was by jet engine spark plug.

The entrance to the test section was located at the end of the mixing chamber. As shown in figure 2, the test section was made up of a heavy wall pipe and a thin inner liner or insert. Figure 4 shows the details of the insert. The 304 stainless-steel inner liner wall thickness of 0.010 inch (0.254×10^{-3} m) would not support the required pressures;

3
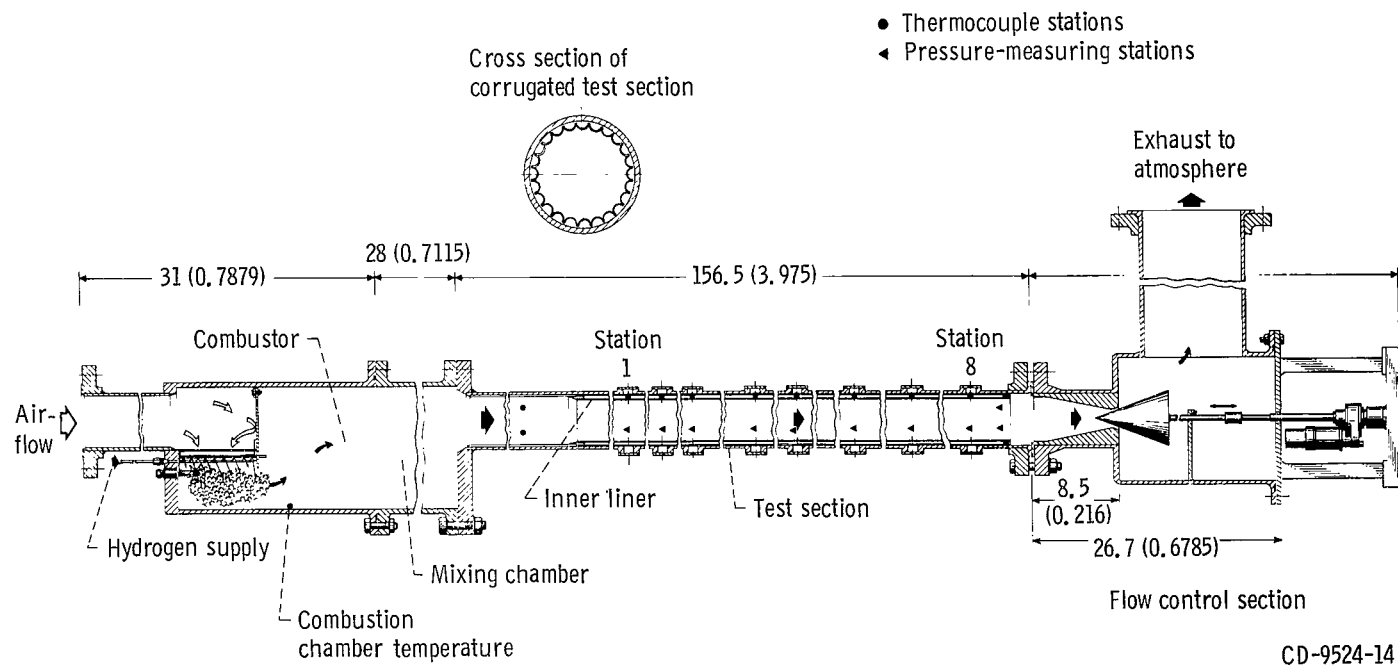
Figure 2. - Apparatus for determining convective heat transfer between simulated rocket cooling tubes. Dimensions are in inches (m).

Air supply

Hydrogen injection tube

Spark plugs

Section A-A

Mixture of hot air and water vapor

Supply air turning baffle

A

A

Airflow

Spark plugs

Hydrogen supply

Baffle plate

10-in. (0.254-m) heavy wall pipe

CD-9610-14

Figure 3. - Combustor detail.

Test section total
temperature sur-
vey rake A-A

Thermocouple
location B-B

Test section total-
pressure survey
rake D-D

4.37 in.
(0.111 m)

1 in.
(0.0254 m)

Thermocouple pressure-
tight feedthrough

Airflow

X

A

A

B

B
C

Station 1

Bleed port

Test section support band

Station 8 D

D

C

30°

Station total temperature
thermocouple (air)

Total-pressure rakes

X = 14.7 in.
(0.3733 m)

X = 154.25 in.
(3.919 m)

CD-9611-14

Boundary layer survey
rake installation C-C

(a) Corrugated test section. Wall thickness, 0.010 inch (0.000254 m); 304 stainless steel.

Figure 4. - Corrugated and smooth-wall sections.

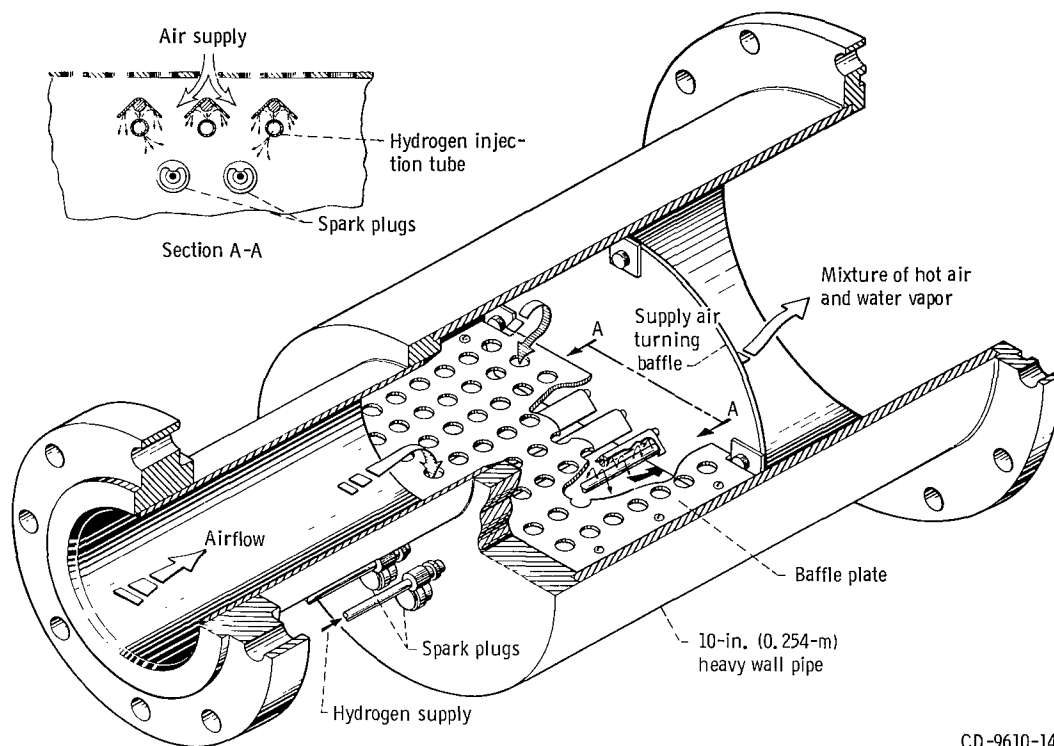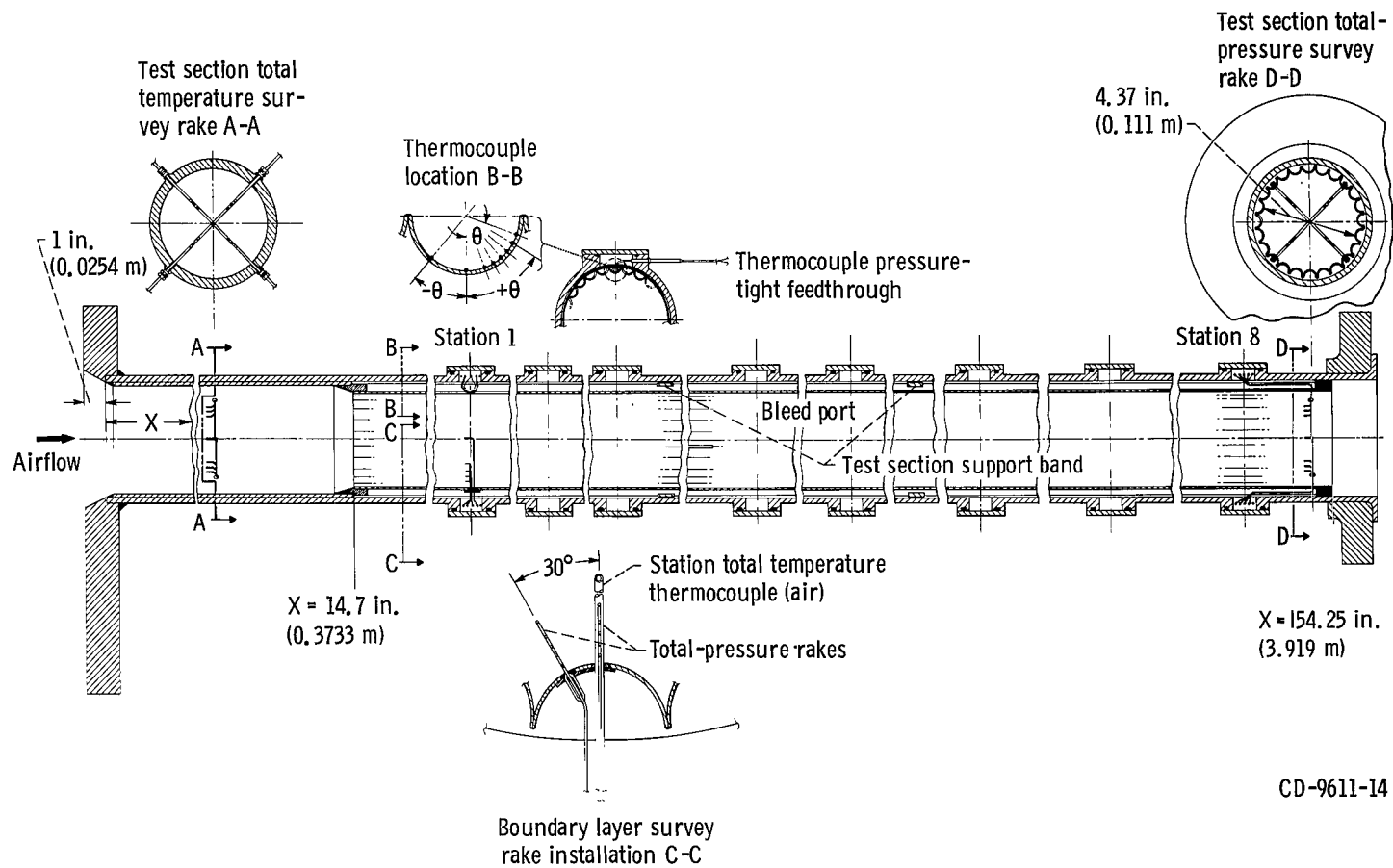(b) Smooth-wall test section insert. Wall thickness, 0.010 inch (0.000254 m); 304 stainless steel.
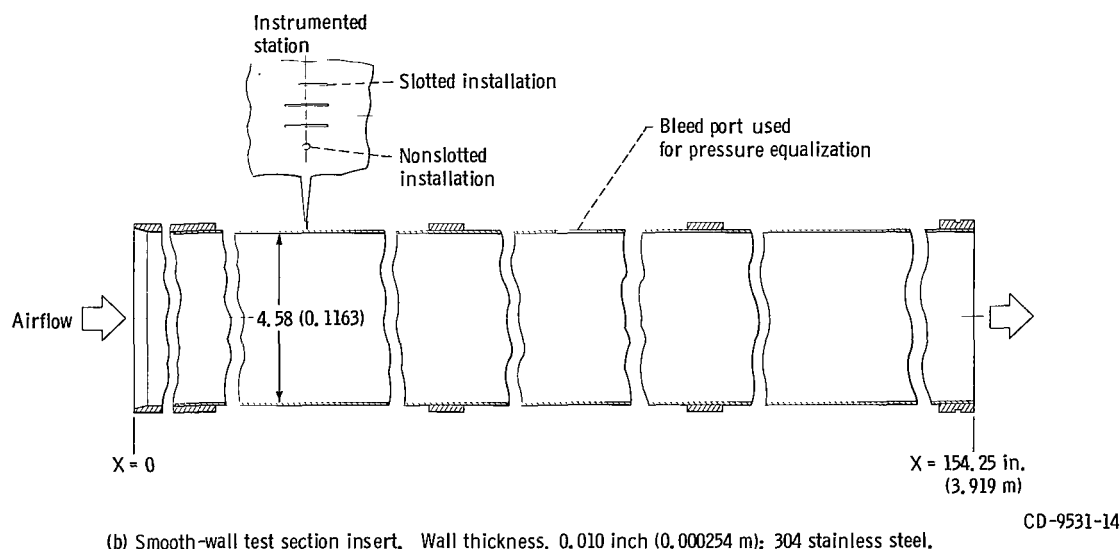
CD-9531-14

Figure 4. - Concluded.

hence, the insert was vented and the heavy gage pipe was used to withstand the pressure forces. Two insert configurations were built. Figure 4(a) shows the corrugated insert (inside tube to tube diameter, 4.37 in. (0.111 m)) which simulates the rocket wall. The diameter of the simulated cooling tube was 5/8 inch (0.01588 m). Figure 4(b) shows the smooth wall insert (i.d., 4.58 in. (0.1163 m)) which was used for comparison. The corrugated insert had a smooth section at its entrance which then made a transition to the corrugated section upstream of the first measuring station. The smooth wall insert did not require a transition section.

The mass flow rate metering plug was located downstream of the test section as shown in figure 2. The plug could be moved into the pipe thus restricting the mass flow rate. The pressure ratio across the plug insured choking at the minimum flow area. Knowing this area as a function of plug travel along with measured total pressure and temperature provides enough information to calculate the mass flow rate past the plug. This mass flow rate agreed with the mass flow rate measured by an orifice located in the piping leading to the combustor.

INSTRUMENTATION

Operating Instrumentation

The instrumentation used in the operation of the rig consisted of a combustor temperature thermocouple located between the combustor and mixing chamber, total tem-

7

perature survey rakes located just downstream of the test section entrance, and total pressure survey rakes located at the test section exit just upstream of the mass flow rate metering plug. Each of the measuring points in the survey rakes were located by dividing the area of the passage by 4, assuming the flow to be symmetrical about the centerline and assigning each of the four equal areas to the included area between two concentric circles. The temperature or pressure sensor was then placed at a point in the included area such that a circle drawn through the sensor divides the included area in half. This gives an area weighting to the measurements. The centerline sensor was assumed to read the average reading for the area assigned to it. The thermocouples were read from a self-balancing potentiometer. The pressures were measured using mercury manometer boards and recorded by photographing the boards.

Test Section Instrumentation

The calculation of the heat-transfer coefficient requires the measurement of the phase lag between the free-stream air temperature and the wall temperature. To measure the free-stream temperature, a thermocouple made of Chromel-Alumel wires (0.007-in. (0.000178-m) diam) having an exposed bead diameter of 0.007 inch (0.000178 m) was built. This thermocouple was located at the centerline of the test section and at the same axial distance as the wall temperature measuring station (fig. 5). The wall temperatures were measured using Chromel-Alumel 0.001-inch (0.0254×10^{-3}-m) diameter thermocouple wire. Two types of installation were made using these wires. One type of installation is shown in figure 5, where thermocouple wires are spot-welded in the bottom center of a 0.010 inch (0.254×10^{-3} m) slot ground to a depth of half the wall thickness, 0.005 inch (0.127×10^{-3} m). A small drop of high temperature cement attached the wires to the wall away from the spot weld. The second method of installation was simply to spot-weld the wires to the back of the wall. The high temperature cement was again used to hold the wire in place. This prevented the wire from vibrating and breaking at the spot weld (which tests showed to be a problem).

Wall temperatures were measured at the stations shown in figure 2. The axial distances X from the entrance to the stations are tabulated in table II. At each station the wall temperatures were measured at different points around the simulated cooling tube. The angular location θ of these points is shown in figure 4(a) for the corrugated test section and are tabulated in table II. This test section used the slot-type installation only. The smooth-wall test section used both types, as shown in figure 4(b).

The thermocouple reference junction was immersed in boiling water (212° F (373 K)). A switching arrangement allowed the air temperature plus all the wall temperatures at a station to be read into a galvanometer type strip chart. To ensure the same response and electrical phase lags of the air and wall temperature galvanometers the line resis-
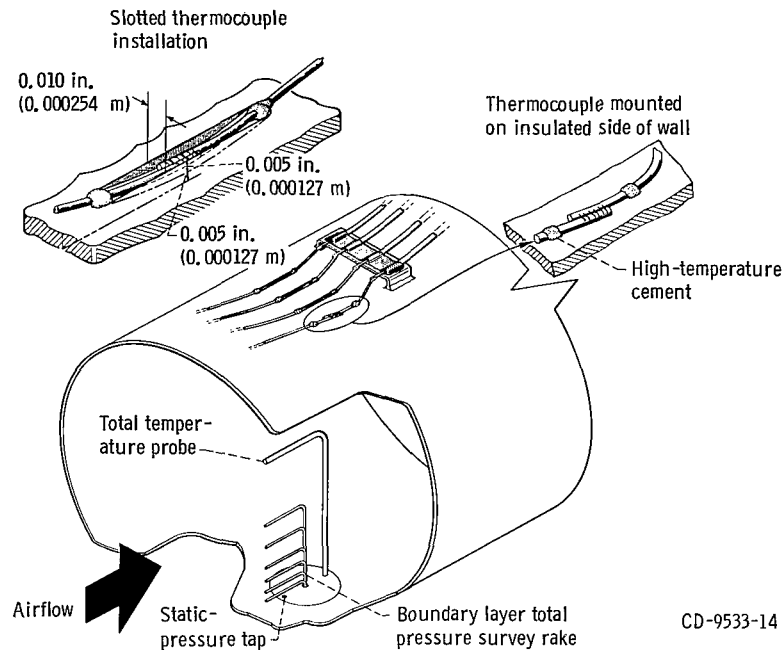
Figure 5. - Instrumentation installed in smooth-wall test section.

tance of each thermocouple was adjusted to 350 ohms. This resistance was required so that the phase shift between input and output of the galvanometers become linear with frequency. This then allows comparisons which are independent of frequency. The frequency range covered in the experiment was less than 0.1 of the natural frequency of the galvanometers.

Boundary layer total pressure survey rakes were constructed as shown in figure 5. These were located at each station. The corrugated test section had two rakes at each station, as shown in figure 4(a) cross section C-C. A static pressure tap was also located at each station. These pressures were measured using mercury manometer boards and were recorded by photographing the boards. The boards were referenced to the combustion chamber pressure which was read from a Bourdon-type pressure gage accurate to 0.5 psi ($3.447{\times}10^3$ kN/m^2).

DATA REDUCTION AND PROCEDURE

The method used to determine the convective heat transfer coefficient h is developed in reference 3. It consists in this case of sinusoidally oscillating the temperature of the air flowing through the insulated test section and measuring the response of the wall temperature. The phase lag between the air and wall temperatures along with the

wall properties (i.e., density, specific heat, thermal conductivity) and frequency of the air temperature oscillations can be used to calculate the convective heat-transfer coefficient h. The location of the wall temperature sensor must also be known if the thermal conductivity is an important factor. The equation used to calculate the convective heat-transfer coefficient h is taken from reference 3 for the temperature measured at the insulated side of the wall x = L. The equation is

$$\frac{h}{K\eta} = \frac{1 - e^{2\eta L}(\cos 2\eta L + \sin 2\eta L) - \overline{CON}\left[e^{2\eta L}(\cos 2\eta L - \sin 2\eta L) - 1\right]}{e^{2\eta L} \sin 2\eta L + \overline{CON}(e^{2\eta L} \cos 2\eta L + 1)} \tag{1}$$

where

$$\overline{CON} = \tan(\varphi = \eta L)$$

$$\eta = \sqrt{\frac{\omega}{2\alpha}}$$

Symbols are defined in the appendix. The phase shift φ is <0 for the wall temperature lagging the fluid temperature.

Table I lists the material properties at 960° R (533 K) for 347 stainless steel which are assumed equal to those of 304 stainless steel. Table II lists the test conditions including the driving frequency f, phase shifts, and the calculated heat-transfer coefficients.

The procedure for determining the phase lag was to record the free-stream air temperature and all the wall temperatures at a selected station on a strip chart while oscillating sinusoidally the hydrogen flow to the combustor. The frequency (0.05 Hz) of the oscillation was picked to give adequate phase lags for the h existing in the test section. The phase lags were measured from the strip chart as follows.

First, the point where each sine wave (temperature plot) goes through its zero point (the point where the temperature was equal to the maximum temperature minus the minimum divided by 2) was determined. Then the distance, on the time axis, between this point on the air temperature curve and the point on the wall temperature curve was measured. This distance divided by the distance traveled by the chart during one period multiplied by 360° is the phase lag in degrees. This was used along with the wall properties taken at the mean wall temperature (table I) and the frequency of air temperature oscillation (0.05 Hz) to calculate h from equation (1).

The desired total pressure in the test section was set using an upstream throttling valve and was measured using the pressure tap in the combustor. The test section total

temperature was set by adjusting the hydrogen flow to the combustor and was measured using the thermocouples located just downstream of the test section inlet. The mass flow rate of air through the test section was set by the plug position. The equation used to calculate the mass flow rate was

$$W = \frac{p^*}{P} PA^* \sqrt{\frac{\gamma g}{R \frac{t^*}{T} \overline{T}}} \tag{2}$$

This equation assumes a one-dimensional flow of an ideal gas, an isentropic process, a flow coefficient of 1, and that the flow was choked at the plug. An approximate mass flow rate of 10.12 pounds per second (4.590 kg/sec) was selected for the tests so that the Reynolds number based on the smooth tube test section inside diameter was 1.78×10^6, thus ensuring turbulent flow.

The pressures taken from the boundary layer survey rakes and test section total temperature were used along with the measured static pressure at the station to calculate the velocities using the following equation:

$$v = \sqrt{2gR\overline{T}\frac{\gamma}{\gamma - 1}\left[1 - \left(\frac{p}{P}\right)^{(\gamma-1)/\gamma}\right]} \qquad \text{(Isentropic, adiabatic, perfect gas)} \tag{3}$$

For these calculations the measured static pressure was assumed to be constant across the duct.

RESULTS AND DISCUSSION

Table II shows the test condition and data. The weight flow rate through the test section was held approximately constant at 10.12 pounds per second (4.590 kg/sec). The total pressure was set at about 149 psia (1023 kN/m^2). The total temperature was set at 960° R (533 K).

Table III lists the static and total pressures which were measured in the test sections. Figure 6 shows the difference between the measured total and static pressure as a function of axial distance. The distributions are shown for both the corrugated and smooth-wall test sections. The corrugated test section was rippled, due to the test section support band (fig. 4(a)), near stations 3 and 6 (X = 60.5 in. (1.524 m) and 114.5 in. (2.655 m), respectively). This may account for the lower pressure differences at these stations compared with the other data. The axial variation of the pressure differences
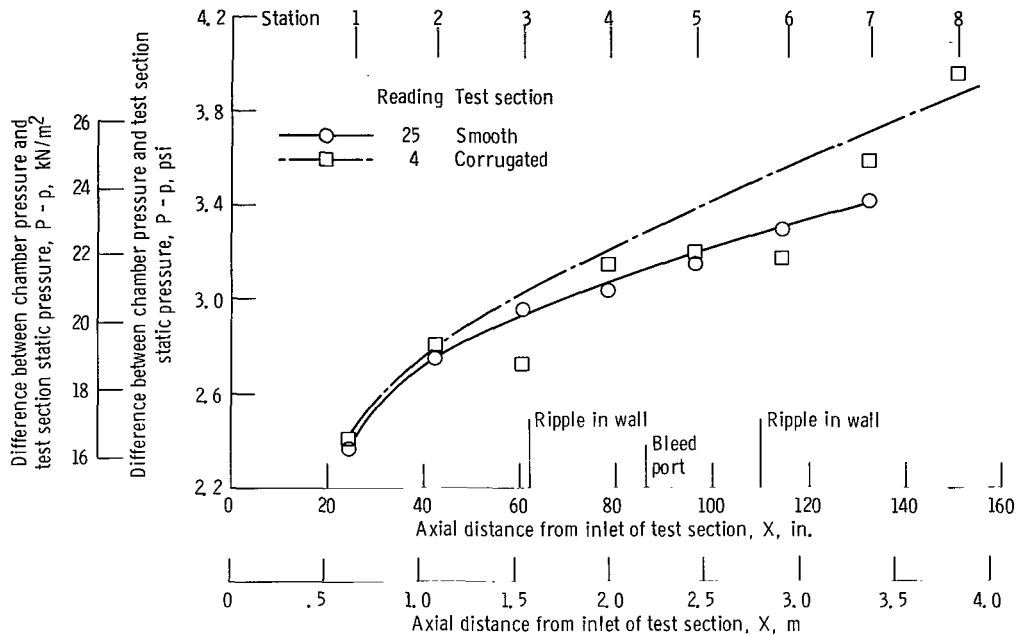
Figure 6. - Difference between combustion chamber pressure and test section static pressure, as function of axial distance.

(free-stream maximum velocity indicator) for both test sections seem to be about the same at the early stations. A deviation exists at the latter stations which indicates a higher free-stream velocity in the corrugated test section. The data scatter for the corrugated test section is somewhat larger than that of the smooth-wall test section.

The boundary layer velocity profile in terms of the simulated rocket cooling tube radius r used in the corrugated test section is shown in figure 7. The data are calculated using the total and static pressures measured by the survey rakes shown in figures 4(a) and 5.

The boundary layer thickness based on 99 percent of the smooth-wall, free-stream velocity is approximately 1.8 times the simulated rocket tube radius (y/r = 1.8, fig. 7). Since the survey rakes for the corrugated test section did not extend far enough into the stream, it can only be said that the boundary layer thickness is greater than y/r = 1.0 and is probably greater than y/r = 1.8.

The slope of the profile for the smooth wall increases faster with radial distance than that of the corrugated wall for values of y/r > 0.4. This indicates that the boundary layer interaction that is viscous turbulent mixing between the tubes of the corrugated test section causes the boundary layer to grow more rapidly than that of the smooth-wall test section. Because the displacement thickness is larger in the case of the corrugated wall, the free-stream velocity must be larger than that of the smooth wall in order to pass equal weight flows. Judging from the relative slope of the velocity profiles this is the case.

12

Reading Station Axial distance from Test section Rake at –
inlet of test section, deg (rad)
in. (m)

Reading	Station	Axial distance in.	from inlet (m)	Test section	Rake at deg	– (rad)
13	4	78.5	(1.994)	Smooth	--	-------
13	5	96.5	(2.452)	Smooth	--	-------
4	4	78.5	(1.994)	Corrugated	0	(0)
	5	96.5	(2.452)		0	(0)
4	4	78.5	(1.994)		30	(0.2619)
	5	96.5	(2.452)		30	(0.2619)
	1	24.5	(.622)		0	(0)
	2	42.5	(1.080)		0	(0)
	3	60.5	(1.537)		0	(0)
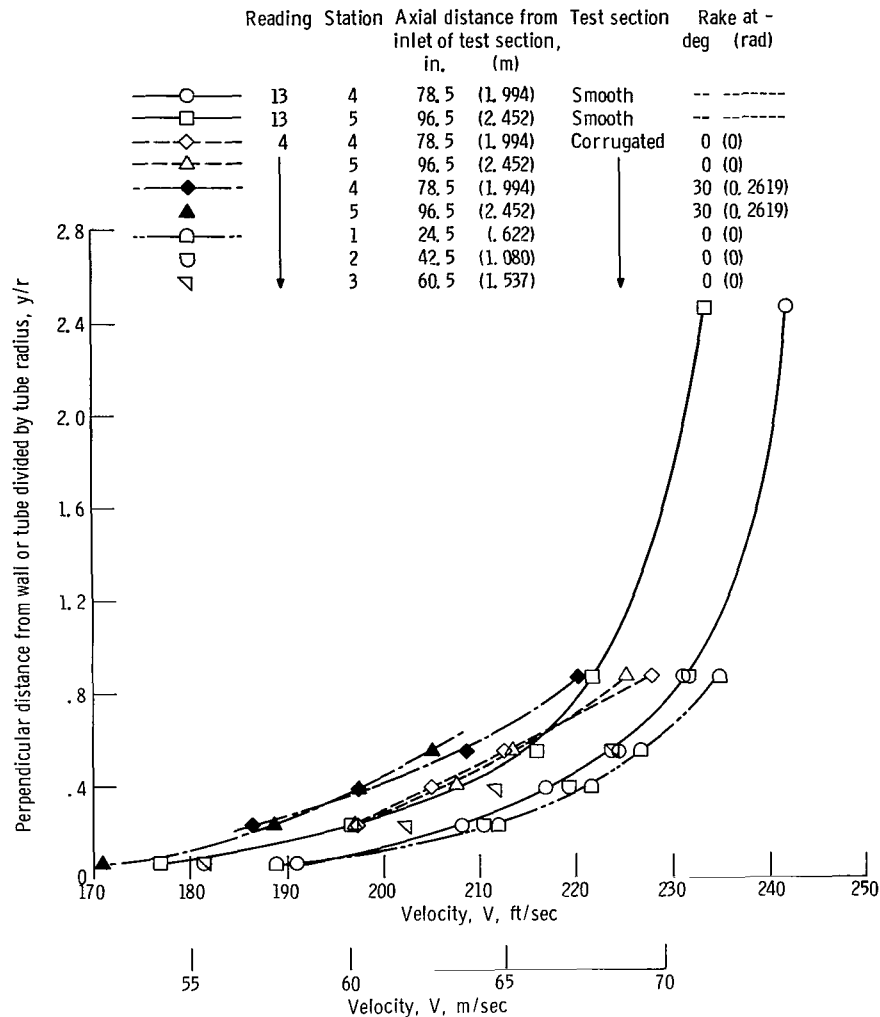
Figure 7. – Comparison of boundary layer profiles for smooth and corrugated test sections
as function of axial distance. Radius of simulated rocket cooling tube, 5/16 inch
(0.794 cm).

The 30° rake (fig. 4(a)) measures lower velocities than the 0° rake, as would be expected if the boundary layer filled the area between the tubes.

As shown in figure 5, the wall temperatures were measured using two types of thermocouple installations; one in which the thermocouple was placed on the insulated surface of the thin (0.010 in. (0.254×10^{-3} m)) wall and the other that placed the thermocouple in the center of a slot having half the wall thickness depth and equal to the wall thickness in width. The heat-transfer coefficient h for both types was calculated using equation (1) which assumes that the sensor is located at the insulated face of the tube (x/L = 1). This is permissible because, as shown in reference 3, thin walls (0.010 in. (0.254×10^{-3} m)) have small (2.6 percent) errors with regard to sensor location. Com-

13

Figure 8. - Heat-transfer coefficient as function of axial distance. Smooth-wall test section; reading 19; forcing frequency, 0. 05 hertz.

parison of the measured phase lags for the two types verified this. This, then, justifies the use of equation (1) in calculating h for either type thermocouple installation. The slotted type was used on the corrugated test section. Both types were used on the smooth-wall test section.
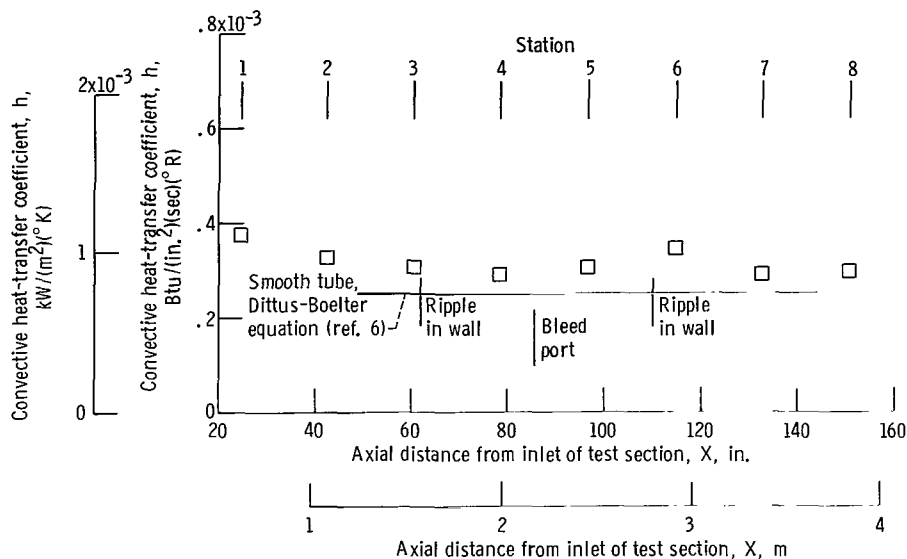
Figure 8 shows the heat-transfer coefficient as a function of axial distance for the smooth-wall test section. The Dittus-Boelter equation (ref. 6) gives a value of 0.25×10^{-3} Btu/(in.^{2})(sec)(^{O}R) (0. 736 kW/(m)(K)). This agrees within 20 percent of the measured value at $X > 70$ inches (1. 78 m).

Figure 9 shows the variation of the convective heat-transfer coefficient as a function of axial distance for the corrugated test section. The data is shown for two circumferential tube locations, $\theta = 0^O$ and 20° (0. 349 rad). As would be expected, the h decreased with axial distance. The comparison of data for runs 4 and 5 show a ±20 percent scatter, with the exception of station 6. Station 6, as well as station 3, had ripples in the tube close by, caused by the test section support bands shown in figure 4(a). These ripples, which may have been caused by differential expansion between the band and thin wall tubes, may explain the larger scatter in the data at station 6. No data were taken at station 3 due to thermocouple breakage.

A comparison of the heat transfer coefficients for the corrugated wall and the smooth wall is shown in figure 10. The ratio of the heat transfer coefficients $(h_{corrugated}/h_{smooth})$ as a function of axial distance is plotted. The data fall within a ±20 percent scatter band, with the exception of station 6 which had rippled tubes as previously noted. The conclusion, then, is that within a ±20 percent scatter band the con-

Reading Angular displacement, Forcing frequency,
θ,   f,
deg   (rad)   Hz

4   0   (0)   0.05
4   20   (0.349)
5   0   (0)
5   20   (.349)

Station 1 2 3 4 5 6 7 8

Ripple in wall

Ripple in wall

Bleed port

Convective heat-transfer coefficient, h, kW/(m²)(°K)

Convective heat-transfer coefficient, h, Btu/(in.²)(sec)(°R)

Axial distance from inlet of test section, X, in.

Axial distance from inlet of test section, X, m
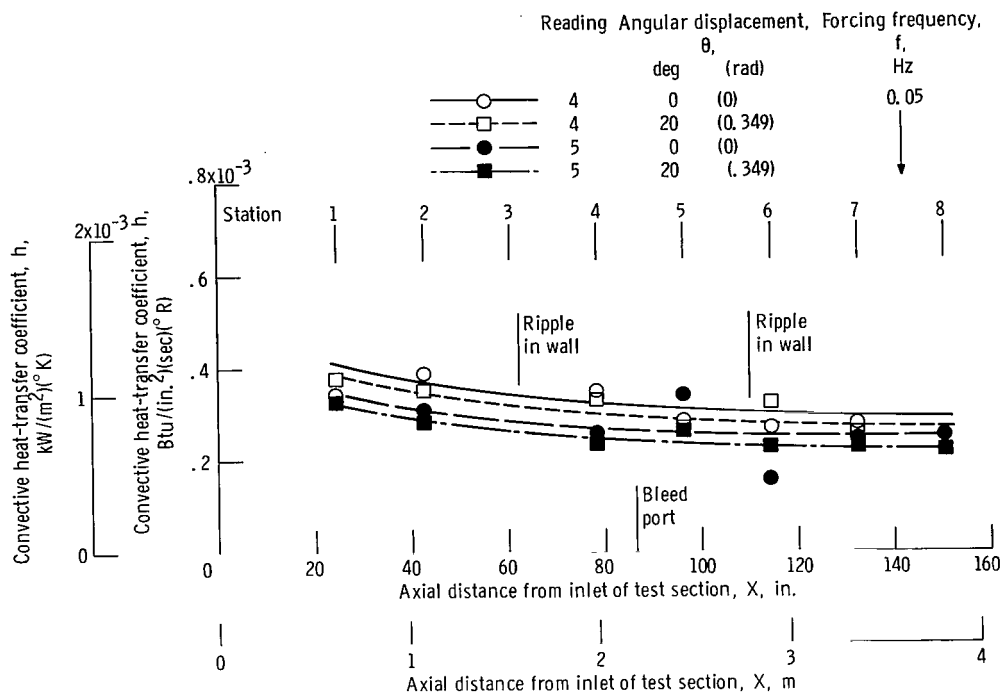
Figure 9. - Effect of axial distance on convective heat-transfer coefficient in corrugated test section.

Reading Angular displacement, Forcing frequency,
θ,   f,
deg   Hz

○   4   0   0.05
●   5   0   .05

Station 1 2 3 4 5 6 7 8

Ratio of convective heat transfer for corrugated test section to that in smooth test section, $h_{corrugated}/h_{smooth}$

Axial distance from inlet of test section, X, in.

Axial distance from inlet of test section, X, m

Figure 10. - Comparison of heat-transfer coefficients for corrugated test section (θ = 0°) with those of smooth wall (reading 19), as function of axial distance.
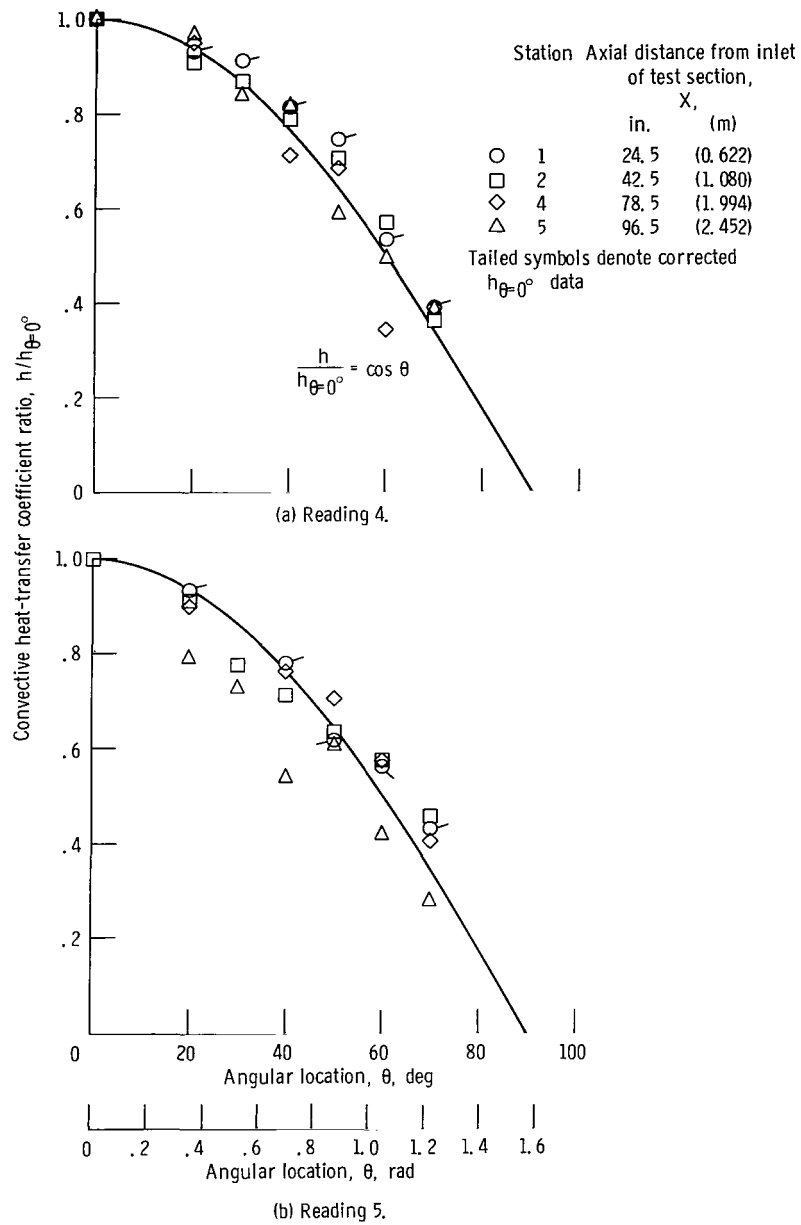
Figure 11. - Variation of convective heat-transfer coefficient with circumferential displacement. Forcing frequency, 0.05 hertz.

vective heat-transfer coefficients for the smooth wall are the same as those on the corrugated wall at $\theta = 0^{\circ}$.

The peripheral variation of the convective heat-transfer coefficient is shown in figure 11. The ratio of the convective heat-transfer coefficient at a given circumferential location to that at the crest ($\theta = 0$) is plotted as a function of the circumferential location.

As Deissler's work (ref. 2) indicates, the heat-transfer coefficient is a maximum at the crest and approaches zero between the tubes. The cosine curve shown in figure 11 fits the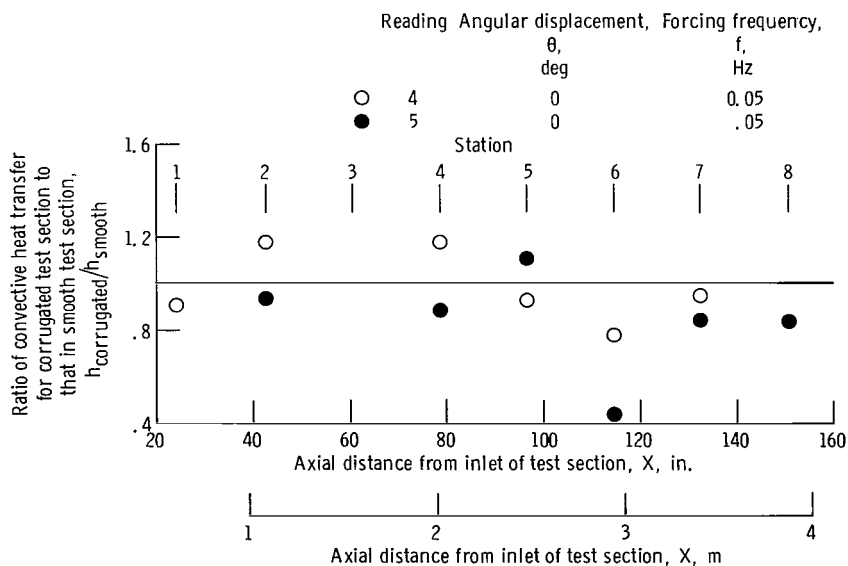 data rather well. Assuming that the results of this test apply to a cooled wall allows the use of the projected area of the cooling tube (tube diameter) to be used as a first approximation, along with the value of the heat-transfer coefficient at the crest ($\theta = 0$), when calculating the heat passed to the coolant in a rocket engine. The latter statement assumes a constant wall temperature or a negligible variation in wall temperature due to the fin effect.

The data covers four of the eight axial positions and is typical of other stations. Data were taken from two separate runs: figure 11(a) presents the data from run 4, while figure 11(b) shows that from run 5. Both runs were at the same test conditions. These two runs are shown for comparison purposes and to show the reproducibility of the data. The tailed symbols denote data where $h_{\theta=0}$ was obviously bad and not usable in the $h/h_{\theta=0}$ ratio. The data for $h_{\theta=20}{}^{\circ}$ was used to calculate a new $h_{\theta=0}{}^{\circ}$ in these cases using $h_{\theta=0}{}^{\circ} = h_{\theta=20}{}^{\circ}/\cos 20^{\circ}$. The $h/h_{\theta=0}{}^{\circ}$ ratios for other circumferential locations θ were then calculated using this calculated $h_{\theta=0}{}^{\circ}$ and the measured data.

CONCLUDING REMARKS

There are two ways in which the cosine variation of the convective heat-transfer coefficient may be used in analyzing heat transfer in rocket engines. The first is to neglect the surface wall temperature drop due to conduction through the wall in the peripheral direction (i. e., fin effect). This may be justified if the hot gas temperature is very large compared to the wall temperature because then the driving temperature difference may not vary appreciably. If this is the case, the cosine variation would allow the use of the projected area of the tube together with the coefficient and wall temperature at the crest of the tube for the calculation of the approximate heat flux to the coolant. The crest coefficient can be calculated from an applicable smooth-wall correlation. A heat balance across the tube will yield the smooth-wall temperature, which would be assumed to be the tube wall temperature at the crest. This procedure is now in use in the regeneratively cooled rocket heat-transfer field but until now has not been experimentally verified.

The second use of the cosine variation of the heat-transfer coefficient in regeneratively cooled rocket engines is as a boundary condition when solving either analytically or

numerically for the wall temperature distribution throughout the tube. A detailed discussion of this, however, is beyond the scope of this report.

The boundary layer interaction between cooling tubes appears to have caused a significant change in the boundary layer velocity profile compared to the profiles for the smooth wall (fig. 7). This may mean that the boundary layer buildup on an axially corrugated wall will tend to fill the region between the tubes rapidly. Consequently, a shorter boundary layer starting length may be needed to develop the cosine variation than might be expected from considerations of a smooth tube entrance effect or boundary layer growth.

In applying the results of this experiment to a rocket engine, it is necessary to allow sufficient boundary layer starting length so that the cosine variation has developed. Since this starting length has not been determined herein, a cautious use of the cosine variation is recommended. However, it would be expected that, in the convergent section of the engine where the volume between the cooling tubes is decreasing, the cosine variation should be applicable. Past the throat region where the engine wall begins to diverge and the boundary layer shock interaction can be expected to disrupt the low energy fluid between the tubes, the validity of the cosine variation may be questioned. The use of the cosine variation in this region may be valid if the engine wall does not diverge more rapidly than the boundary layer can fill the volume between the cooling tubes.

Further work is needed to determine the boundary layer starting length required to develop the cosine variation of the coefficient and the effect of peripheral wall temperature variation due to wall cooling.

SUMMARY OF RESULTS

An experimental program was conducted to find the variation in the gas-side convective heat-transfer coefficient for geometrically simulated rocket cooling tubes having semicircular cross section. The Reynolds number was 1.786×10^6, and the Nusselt number was 2372 (based on the equivalent smooth wall i.d. of the test section). The simulated rocket wall was made using 0.625-inch (0.01588-m) diameter tubing D_{tube}. The first station was located at an axial distance ratio X/D_{tube} of 39.2 and the last at 240.8.

The boundary layer height was approximately equal to the diameter of the simulated cooling tube. The convective heat-transfer coefficient at the crest of the simulated cooling tube was approximately equal to the one measured in a smooth wall. The peripheral variation of the coefficient was proportional to the cosine of the angle measured from the crest of the simulated cooling tube $h/h_{\theta=0}\text{o} = \cos \theta$. This permits the use of the projected area (i.e., diameter) of the cooling tube and the heat transfer

coefficient at the crest in calculating the total heat transfer to the coolant. For this calculation, it is assumed that the wall temperature is constant.

APPENDIX - SYMBOLS

A^* — minimum flow area at flowmetering plug (choked area), $in.^2$; m^2

a — velocity of sound, $\sqrt{\gamma g R t}$, ft/sec; m/sec

c — heat capacity of wall material, Btu/(lb)(^{O}R); J/(kg)(K)

c_p — heat capacity of air at constant pressure, Btu/(lb)(^{O}R); J/(kg)(K)

c_v — heat capacity of air at constant volume, Btu/(lb)(^{O}R); J/(kg)(K)

D_{tube} — diameter of simulated rocket cooling tube, 0.625 in.; 0.01588 m

f — frequency at which air temperature is oscillated, Hz

g — gravitational constant, 32.16 ft/sec^2; 9.8023 m/sec^2

h — convective heat-transfer coefficient on surface of wall, Btu/$(in.^2)$(sec)(^{O}R); $W/(m^2)$(K)

K — thermal conductivity, Btu/(in.)(sec)(^{O}R); J/(m)(sec)(K)

L — thickness of wall (test section wall thickness, 0.010 in.; 0.254×10^{-3} m)

M — Mach number, V/a

P — combustion chamber pressure (total pressure), psia; N/m^2

P_R — average total pressure from test section survey rake, psia; N/m^2

p — static pressure in test section, psia; N/m^2

R — universal gas constant divided by molecular weight (in this case molecular weight of air), 53.3 ft/^{O}R; 29.23 m/K

r — radius of simulated rocket cooling tube, 5/16 in.; 0.7945 cm

T — total temperature, ^{O}R; K

$\overline{T}$ — average total temperature in test section, ^{O}R; K

T_o — combustor total temperature, ^{O}R; K

t — static temperature, ^{O}R; K

V — air velocity, ft/sec; m/sec

$\dot{w}$ — total mass flow rate of air and hydrogen through metering plug, lbm/sec; kg/sec

X — axial distance measured from the entrance of the test section (see figs. 2 and 4(a)), in.; m

x — distance into test section wall measured from convective heat-transfer surface, in.; m

y   perpendicular distance from wall, in.; m

α thermal diffusivity, $K/\rho c$, in.^{2}/sec; m^2/sec

γ ratio of heat capacities, c_p/c_v (1. 4 for air)

θ angular location, deg; rad

π constant, 3. 1416

ρ density of wall material, lb/in.^{3}; kg/m^3

ω angular velocity of temperature oscillation, $2\pi f$, rad/sec

Superscript:

*   indicates choking conditions (i. e., M = 1. 0)

REFERENCES

1. Schacht, Ralph L.; Quentmeyer, Richard J.; and Jones, William L.: Experimental Investigation of Hot-Gas Side Heat-Transfer Rates for a Hydrogen-Oxygen Rocket. NASA TN D-2832, 1965.

2. Deissler, Robert G.; and Taylor, Maynard F.: Analysis of Axial Turbulent Flow and Heat Transfer Through Banks of Rods or Tubes. Reactor Heat Transfer Conference of 1956. USAEC Rep. TID-7529 (pt. 1), bk 2, Nov. 1957, p. 416.

3. Huff, Ronald G.: Determination of Convective Heat-Transfer Coefficients on Adiabatic Walls Using a Sinusoidally Forced Fluid Temperature. NASA TM X-1594, 1968.

4. Anon.: Properties of Some Metals and Alloys. International Nickel Co., Inc., New York, 1951.

5. Tebo, F. J.: Selected Values of the Physical Properties of Various Materials. Rep. ANL-5914, Argonne National Lab., Sept. 1958.

6. Gebhart, Benjamin: Heat Transfer. McGraw-Hill Book Co., Inc., 1961, p. 202.

TABLE I. - MATERIAL PROPERTIES

AT TEST CONDITIONS

[347 Stainless steel, 0.010 in. (0.254×10^{-3} m) at 960° R (533 K).]

Heat capacity, c (ref. 5):	
Btu/(lb)(°R)	0.1263
J/(kg)(K)	0.529×10^3
Thermal conductivity, K (ref. 5):	
Btu/(in.)(sec)(°R)	0.000243
J/(m)(sec)(K)	18.17
Density, ρ (ref. 4):	
lbm/in.^{3}	0.29
kg/m^3	8.03×10^3

TABLE II. - RUNNING CONDITIONS AND .

(a) Corrugated

(a-1) U.S.

Reading	Station	Axial distance, X, in.	Air mass flow rate, $\frac{lbm}{sec}$	Combustion chamber pressure, psia	Combustion chamber temperature, °R	Temperature forcing frequency, f, Hz	Combustion temperature amplitude, °R	0		20	
								Phase shift, deg	Heat-transfer coefficient, h, $\frac{Btu}{(in.^2)(sec)(°R)}$	Phase shift, deg	Heat-transfer coefficient, h, $\frac{Btu}{(in.^2)(sec)(°R)}$
4	1	24.5	10.17	151.2	960	0.05	±50	-18.90	0.339×10^{-3}	-17.28	0.373×10^{-3}
	2	42.5						-16.74	.386	-18.36	.349
	4	78.5						-18.54	.346	-19.44	.328
	5	96.5						-22.32	.282	-23.04	.272
	6	114.5						-23.40	.267	-19.80	.322
	7	132.5						-22.68	.277	-24.48	.254
5	1	24.5	10.12	148.4	960	0.05	±50	-8.82	0.753×10^{-3}	-19.80	0.322×10^{-3}
	2	42.5						-20.70	.307	-22.50	.279
	4	78.5						-24.30	.256	-26.64	.231
	5	96.5						-18.90	.339	-23.40	.267
	6	114.5						-36.72	.155	-27.00	.227
	7	132.5						-25.20	.246	-27.00	.227
	8	150.5						-24.84	.250	-28.08	.217

Reading	Station	Axial distance, X, m	Air mass flow rate, $\frac{kg}{sec}$	Combustion chamber pressure, $\frac{kN}{m^2}$	Combustion chamber temperature, K	Temperature forcing frequency, f, Hz	Combustion temperature amplitude, K	0.02		0.349	
								Phase shift, rad	Heat-transfer coefficient, h, $\frac{kW}{(m^2)(K)}$	Phase shift, rad	Heat-transfer coefficient, h, $\frac{kW}{(m^2)(K)}$
4	1	0.622	4.613	1042.5	533	0.05	±27.8	0.330	0.997	0.302	1.097
	2	1.080						.292	1.136	.321	1.027
	4	1.994						.324	1.018	.339	.965
	5	2.452						.390	.830	.402	.800
	6	2.909						.409	.786	.346	.947
	7	3.365						.396	.815	.428	.747
5	1	0.622	4.590	1023.2	533	0.05	±27.8	0.154	0.346	0.346	0.947
	2	1.080						.361	.903	.393	.821
	4	1.994						.424	.753	.465	.677
	5	2.452						.330	.997	.409	.786
	6	2.909						.641	.456	.472	.668
	7	3.365						.440	.724	.472	.668
	8	3.823						.434	.736	.490	.638

TABULATED HEAT-TRANSFER DATA

test section

customary units

Angular location, θ, deg									
30		40		50		60		70	
Phase shift, deg	Heat-transfer coefficient, h, $\frac{Btu}{(in.^2)(sec)(^\circ R)}$	Phase shift, deg	Heat-transfer coefficient, h, $\frac{Btu}{(in.^2)(sec)(^\circ R)}$	Phase shift, deg	Heat-transfer coefficient, h, $\frac{Btu}{(in.^2)(sec)(^\circ R)}$	Phase shift, deg	Heat-transfer coefficient, h, $\frac{Btu}{(in.^2)(sec)(^\circ R)}$	Phase shift, deg	Heat-transfer coefficient, h, $\frac{Btu}{(in.^2)(sec)(^\circ R)}$
-17.64	0.365×10^{-3}	-19.62	0.325×10^{-3}	-21.24	0.298×10^{-3}	-28.44	0.213×10^{-3}	-36.36	0.157×10^{-3}
-19.08	.335	-20.88	.304	-23.04	.272	-27.72	.220	-39.6	.140
------	----------	-25.20	.246	-26.10	.236	-44.10	.119	-40.50	.135
-26.10	0.236×10^{-3}	-26.82	.229	-34.92	.165	-39.6	.140	-46.44	.110
-21.60	.292	-26.64	.231	-29.70	.203	-26.1	.236	-49.5	.098
-25.92	.238	-29.70	.203	-33.3	.176	-40.14	.137	-51.84	.091
-19.08	0.335×10^{-3}	-23.40	0.267×10^{-3}	-28.80	0.210×10^{-3}	-30.96	0.193×10^{-3}	-38.16	0.147×10^{-3}
-25.92	.238	-27.90	.218	-30.78	.194	-33.30	.176	-39.42	.140
------	----------	-30.60	.195	-32.58	.181	-38.16	.147	-48.06	.104
-25.20	0.246×10^{-3}	-32.40	.182	-29.34	.206	-39.24	.141	-50.76	.094
-27.90	.218	-32.40	.182	-35.64	.161	-42.12	.128	-51.30	.092
-28.80	.210	-31.86	.186	-37.26	.152	-48.60	.102	-57.24	.074
-29.88	.201	-33.30	.176	-36.90	.154	-43.92	.120	-50.94	.094

(a-2) SI units

Angular location, θ, rad									
0.524		0.698		0.873		1.047		1.222	
Phase shift, rad	Heat-transfer coefficient, h, $\frac{kW}{(m^2)(K)}$	Phase shift, rad	Heat-transfer coefficient, h, $\frac{kW}{(m^2)(K)}$	Phase shift, rad	Heat-transfer coefficient, h, $\frac{kW}{(m^2)(K)}$	Phase shift, rad	Heat-transfer coefficient, h, $\frac{kW}{(m^2)(K)}$	Phase shift, rad	Heat-transfer coefficient, h, $\frac{kW}{(m^2)(K)}$
0.308	1.074	0.343	0.956	0.371	0.877	0.497	0.627	0.635	0.462
.333	.986	.365	.883	.402	.800	.484	.647	.692	.412
-----	-----	.440	.724	.456	.694	.770	.350	.707	.397
0.456	0.694	.468	.674	.610	.485	.691	.412	.811	.324
.377	.859	.465	.680	.519	.598	.456	.694	.864	.288
.452	.700	.519	.598	.582	.518	.701	.403	.905	.268
0.333	0.986	0.409	0.786	0.503	0.618	0.541	0.568	0.666	0.432
.453	.700	.487	.641	.537	.571	.582	.518	.688	.412
-----	-----	.534	.574	.569	.533	.666	.432	.839	.306
0.440	0.724	.566	.535	.512	.606	.685	.415	.886	.277
.487	.642	.566	.535	.622	.474	.736	.377	.896	.271
.503	.618	.556	.547	.651	.447	.849	.300	1.000	.218
.522	.592	.582	.518	.644	.453	.767	.353	.882	.277

25

TABLE II. - Concluded. RUNNING CONDITIONS AND TABULATED HEAT-TRANSFER DATA

(b) Smooth-wall test section

(b-1) U.S. customary units

Reading	Station	Axial distance, X, in.	Air mass flow rate, $\frac{lbm}{sec}$	Combustion chamber pressure, psia	Combustion chamber temperature, °R	Temperature forcing frequency, f, Hz	Combustion temperature amplitude, °R	Phase shift, deg	Heat-transfer coefficient, h, $\frac{Btu}{(in.^2)(sec)(°R)}$
19	1	24.5	10.12	149.2	960	0.05	±50	-17.28	0.373×10^{-3}
	2	42.5						-19.44	.328
	3	60.5						-20.70	.307
	4	78.5						-21.60	.292
	5	96.5						-20.88	.304
	6	114.5						-18.72	.342
	7	132.5						-21.60	.292
	8	150.5						-21.24	.298
[a]25			10.12	149.2	960	0	0		

(b-2) SI units

Reading	Station	Axial distance, X, m	Air mass flow rate, $\frac{kg}{sec}$	Combustion chamber pressure, $\frac{kN}{m^2}$	Combustion chamber temperature, K	Temperature forcing frequency, f, Hz	Combustion temperature amplitude, K	Phase shift, rad	Heat-transfer coefficient, h, $\frac{kW}{(m^2)(K)}$
19	1	0.622	4.590	1028.7	533	0.05	±27.8	0.3017	1.097
	2	1.080						.3394	.965
	3	1.537						.3614	.903
	4	1.994						.3771	.859
	5	2.452						.3645	.894
	6	2.909						.3269	1.006
	7	3.365						.3771	.859
	8	3.823						.3710	.877
[a]25			4.590	1028.7	533	0	0		

[a]This reading is a steady-state case used to determine the static and total pressure in the smooth wall test section.

TABLE III. - TABULATED PRESSURE DATA

(a) Corrugated test section

(a-1) U.S. customary units

Reading	Station	Static pressure, psia	Perpendicular distance, y, in.										Combustion chamber pressure, psi
			0° rake					30° rake					
			0.02	0.07	0.12	0.17	0.27	0.02	0.07	0.12	0.17	0.27	
4	1	148.82	150.45	150.87	151.06	151.17	151.34	------	------	------	------	------	151.22
	2	148.56	150.06	150.58	150.75	150.85	151.01	------	------	------	------	------	
	3	148.50	150.00	150.36	150.54	150.78	150.64	------	------	------	------	------	
	4	148.08	150.29	149.84	149.99	150.13	150.44	151.22	149.65	149.85	150.06	150.28	
	5	148.03	151.22	149.79	149.98	150.09	150.33	149.35	149.64	149.79	149.93	148.09	
	6	148.05	------	------	------	------	------	------	------	------	------	------	
	7	147.64	------	------	------	------	------	------	------	------	------	------	
	8	147.27	------	------	------	------	------	------	------	------	------	------	

(a-2) SI units

Reading	Station	Static pressure, kN/m^2	Perpendiuclar distance, y, mm										Combustion chamber pressure, kN/m^2
			0-radian					5.24-radian rake					
			0.508	1.78	3.05	4.32	6.86	0.508	1.78	3.05	4.32	6.86	
			Rake total pressure, kN/m^2										
4	1	1026.1	1037.3	1040.2	1041.5	1042.3	1043.5	------	------	------	------	------	1042.5
	2	1024.3	1034.6	1038.2	1039.4	1040.1	1041.2	------	------	------	------	------	
	3	1023.9	1034.2	1036.7	1037.9	1039.6	1038.6	------	------	------	------	------	
	4	1021.0	1036.2	1033.1	1034.2	1035.1	1037.3	1042.6	1031.8	1033.2	1034.6	1036.2	
	5	1020.6	1042.6	1032.8	1034.1	1034.8	1036.5	1029.7	1031.7	1032.8	1033.7	1021.1	
	6	1020.8	------	------	------	------	------	------	------	------	------	------	
	7	1017.9	------	------	------	------	------	------	------	------	------	------	
	8	1015.4	------	------	------	------	------	------	------	------	------	------	

TABLE III. - Concluded. TABULATED PRESSURE DATA

(b) Smooth-wall test section

(b-1) U.S. customary units

Read-ing	Sta-tion	Static pressure, psia	Perpendicular distance, y, in.						Combustion chamber pressure, psi
			0.02	0.07	0.12	0.17	0.27	0.77	
			Rake total pressure, psia						
25	1	146.86	------	------	------	------	------	------	149.22
	2	146.48	------	------	------	------	------	------	
	3	146.27	------	------	------	------	------	------	
	4	146.19	147.82	148.13	148.30	148.45	148.59	148.82	
	5	146.08	147.48	147.81	149.22	148.16	148.28	148.52	
	6	145.93	------	------	------	------	------	------	
	7	145.81	------	------	------	------	------	------	

(b-2) SI units

Read-ing	Sta-tion	Static pressure, kN/m^2	Perpendicular distance, y, mm						Combustion chamber pressure, kN/m^2
			0.508	1.78	3.05	4.32	6.86	19.56	
			Rake total temperature, kN/m^2						
25	1	1012.6	------	------	------	------	------	------	1028.7
	2	1010.0	------	------	------	------	------	------	
	3	1008.5	------	------	------	------	------	------	
	4	1008.0	1019.2	1021.3	1022.5	1023.5	1024.5	1026.1	
	5	1007.2	1016.8	1019.1	1028.8	1021.5	1022.4	1024.0	
	6	1006.2	------	------	------	------	------	------	
	7	1005.3	------	------	------	------	------	------	

FIRST CLASS MAIL

POSTMASTER: If Undeliverable (Section 158
Postal Manual) Do Not Return

*"The aeronautical and space activities of the United States shall be
conducted so as to contribute . . . to the expansion of human knowl-
edge of phenomena in the atmosphere and space. The Administration
shall provide for the widest practicable and appropriate dissemination
of information concerning its activities and the results thereof."*

— NATIONAL AERONAUTICS AND SPACE ACT OF 1958

NASA SCIENTIFIC AND TECHNICAL PUBLICATIONS

TECHNICAL REPORTS: Scientific and
technical information considered important,
complete, and a lasting contribution to existing
knowledge.

TECHNICAL NOTES: Information less broad
in scope but nevertheless of importance as a
contribution to existing knowledge.

TECHNICAL MEMORANDUMS:
Information receiving limited distribution
because of preliminary data, security classifica-
tion, or other reasons.

CONTRACTOR REPORTS: Scientific and
technical information generated under a NASA
contract or grant and considered an important
contribution to existing knowledge.

TECHNICAL TRANSLATIONS: Information
published in a foreign language considered
to merit NASA distribution in English.

SPECIAL PUBLICATIONS: Information
derived from or of value to NASA activities.
Publications include conference proceedings,
monographs, data compilations, handbooks,
sourcebooks, and special bibliographies.

**TECHNOLOGY UTILIZATION
PUBLICATIONS:** Information on technology
used by NASA that may be of particular
interest in commercial and other non-aerospace
applications. Publications include Tech Briefs,
Technology Utilization Reports and Notes,
and Technology Surveys.

Details on the availability of these publications may be obtained from:

SCIENTIFIC AND TECHNICAL INFORMATION DIVISION

NATIONAL AERONAUTICS AND SPACE ADMINISTRATION
Washington, D.C. 20546